ISSN 0022-4766, Journal of Structural Chemistry, 2022, Vol. 63, No. 1, pp. 87-99. © Pleiades Publishing, Ltd., 2022.
Russian Text © The Author(s), 2022, published in Zhurnal Strukturnoi Khimii, 2022, Vol. 63, No. 1, pp. 48-60.

MAGNETIC ANOMALIES IN POLYMERIC CHAIN COMPLEXES $Cu(hfac)_2$ WITH SPIN-LABELED DIALKYLPYRAZOLES

G. V. Romanenko[1], S. V. Fokin[1], E. T. Chubakova[1], A. S. Bogomyakov[1,2], and V. I. Ovcharenko[1,2]*

The structures of hexafluoroacetylacetonate complexes of Cu(II)–$Cu(hfac)_2$– with nitroxide radicals $L^{R1/R2}$, where R1 and R2 are alkyl substituents in the 1,3-pyrazole moiety are studied by X-ray crystallography. It is found that solid phases of all $[Cu(hfac)_2L^{R1/R2}]$ are formed by polymeric chains whose common structural motif is a ditopic bridging coordination of paramagnetic ligands in the head-to-head fashion. The study of the temperature structure dynamics and the related change in the temperature dependence of the effective magnetic moment of the complex shows that changes in both R1 and R2 can substantially affect not only the possibility of the appearance of magnetic anomalies on the temperature curve of the effective magnetic moment but also its shape.

DOI: 10.1134/S0022476622010103

Keywords: nitroxide radicals, copper(II) bis(hexafluoroacetylacetonate), crystal structure, magnetic properties.

INTRODUCTION

Studied $[Cu(hfac)_2L^{R1/R2}]$ belong to breathing crystals based on Cu(II) complexes with nitroxide radicals (NRs) which are characterized by reversible structural rearrangements occurring in the solid phase of these compounds upon changes in the temperature and/or pressure. These rearrangements change the spin multiplicity in exchange clusters {>N–•O–Cu^{2+}–O•–N<} or {>N–•O–Cu^{2+}}, which causes the appearance of anomalies in temperature dependence curves of the effective magnetic moment (μ_{eff}) of the compound and specific changes in the EPR spectra [1-7]. In the discussed class of compounds, phase transitions often take place without destructing the crystal, and this makes them valuable objects for a detailed analysis of structural transformations induced by the external action. This fact in turn underlies the development of a specific group of sensors to the external action [8, 9]. A representative group of the studied heterospin compounds is composed of $Cu(hfac)_2$ complexes with NRs containing 1-R-pyrazol-4-yl substituent in the second position of the imidazoline ring of the nitronylnitroxide moiety (L^R, Scheme 1). The experimental database collected so far for these compounds, which contains information about the magnitudes of exchange integrals and structural parameters of exchange clusters, enables one to predict the appearance of spin transitions in the complexes depending on the size and position of the

[1]Institute "International Tomography Center", Siberian Branch, Russian Academy of Sciences, Novosibirsk, Russia; *Victor.Ovcharenko@tomo.nsc.ru. [2]Zelinsky Institute of Organic Chemistry, Russian Academy of Sciences, Moscow, Russia.
Original article submitted July 14, 2021; revised August 4, 2021; accepted August 4, 2021.

alkyl substituent R in the pyrazole ring L^R [1]. The compounds containing an additional substituent R2 in the pyrazole ring (Scheme 1) have been studied much less, although this substitution can lead to nontrivial effects. Thus, for $[Cu(hfac)_2L^{Me/Et}]$ and $[Cu(hfac)_2L^{Et/Me}]$ a reversible solid-phase polymerization/depolymerization reaction was detected (for the first time for heterospin compounds) [6, 7]. A change in the position of R1 and R2 in $L^{Me/Et}$ and $L^{Et/Me}$ resulted in the opposite directions of effects when the crystals were cooled: polymerization of $[Cu(hfac)_2L^{Et/Me}]$ and depolymerization of $[Cu(hfac)_2L^{Me/Et}]$. This fact stimulated us to expand a series of polymeric chain complexes $[Cu(hfac)_2L^{R1/R2}]$ containing alkyl substituents in positions 1 and 3 of the pyrazole ring [10] and examine the temperatureную structure dynamics and magnetic properties of $[Cu(hfac)_2]$ complexes with $L^{R1/R2}$, where R1 and R2 = Me, R1 and R2 = Et, R1 = Me and R2 = *p*-Pr, R1 = *p*-Pr and R2 = Et.

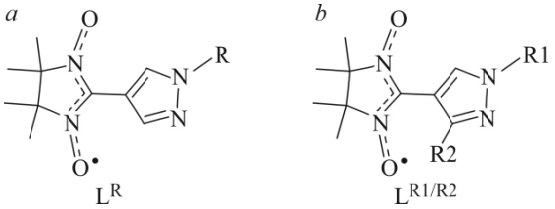

Scheme 1. LR and LR1/R2 NRs.

EXPERIMENTAL

Commercial reagents and solvents were used without additional purification. The reaction course was monitored by thin layer chromatography on Silica gel 60 F254 (Merck) aluminum plates. The chromatographic analysis was conducted on silica gel (0.063-0.200 mm, Merck) for column chromatography. IR spectra (4000-400 cm^{-1}) of nitroxides were recorded on a VECTOR 22 Bruker instrument in KBr pellets. Microanalysis was carried out on a EA-3000 HEKAtech GmbH analyzer. Using the published procedures we synthesized 2,3-bis(hydroxyamino)-2,3-dimethylbutane, 2,3-bis(hydroxyamino)-2,3-dimethylbutane sulfate monohydrate [11], and 2-(1,3-dimethyl-1H-pyrazol-4-yl)-4,4,5,5-tetramethyl-4,5-dihydro-1H-imidazole-3-oxide-1-oxyl ($L^{Me/Me}$) [12]. Other nitroxides used for the synthesis of complexes described below were obtained by Scheme 2 described in detail in [6, 7, 10] and common for dialkyl-substituted NRs.

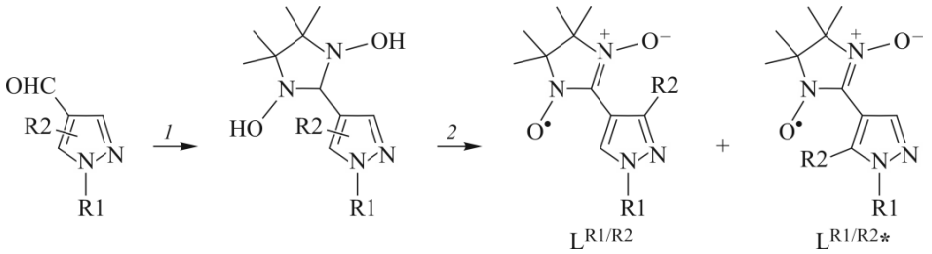

Scheme 2. General synthesis scheme of dialkyl-substituted NRs. 2,3-Bis(hydroxyamino)-2,3-dimethylbutane sulfate monohydrate or 2,3-bis(hydroxyamino)-2,3-dimethylbutane (*1*); $NaIO_4/CH_2Cl_2/H_2O$ or $MnO_2/O_2/CH_3OH$ (*2*).

2-(1,3-diethyl-1*H*-pyrazol-4-yl)-4,4,5,5-tetramethyl-4,5-dihydro-1*H*-imidazole-3-oxide-1-oxyl ($L^{Et/Et}$) and 2-(1-methyl-3-propyl-1*H*-pyrazol-4-yl)-4,4,5,5-tetramethyl-4,5-dihydro-1*H*-imidazole-3-oxide-1-oxyl ($L^{Me/Pr}$) was synthesized from 1,3(5)-diethyl-1*H*-pyrazole and 1-methyl-3-propyl-1*H*-pyrazole-4-carbaldehyde respectively. The formylation procedure, condensation with 2,3-bis(hydroxyamino)-2,3-dimethylbutane, and oxidation were performed as the previously described procedure for $L^{Me/Et}$ [10, 13].

$L^{Et/Et}$. Yield: 88%. According to X-ray crystallography and IR spectroscopy data, during the recrystallization of the product from hexane to the solid phase, dark blue rhombic $L^{Et/Et}$ crystals were isolated. M.p. 92 °C. Found (%): C 59.5, H 7.8,

N 20.0. $C_{14}H_{23}N_4O_2$. Calculated (%): C 60.2, H 8.3, N 20.1. IR spectrum (ν, cm^{-1}): 3444, 3126, 2968, 2931, 2871, 1580, 1506, 1445, 1393, 1352, 1321, 1220, 1173, 1156, 1143, 1111, 1085, 1054, 1014, 956, 871, 847, 802, 761, 728, 698, 654, 608, 540, 500, 464. μ_{eff} = 1.8 μ_B (50-300 K).

$L^{Me/Pr}$. Yield: 95%. According to X-ray crystallography and IR spectroscopy data, during the recrystallization of the product from hexane to the solid phase, blue-purple $L^{Me/Pr}$ crystals were isolated. M.p. 90 °C. Found (%): C 60.4, H 8.1, N 20.0. $C_{14}H_{23}N_4O_2$. Calculated (%): C 60.2, H 8.3, N 20.1. IR spectrum (ν, cm^{-1}): 3418, 3125, 2999, 2961, 2935, 2871, 1583, 1512, 1486, 1458, 1397, 1352, 1291, 1219, 1173, 1154, 1142, 1088, 1004, 895, 871, 839, 774, 747, 710, 654, 642, 638, 609. μ_{eff}= 1.75 μ_B (30-300 K).

$L^{Me/Et}$ and $L^{Et/Me}$ crystals were grown from hexane [6, 7].

[$Cu(hfac)_2L^{Me/Me}$]. A mixture of $Cu(hfac)_2$ (0.0950 g, 0.20 mmol) and $L^{Me/Me}$ (0.0500 g, 0.20 mmol) was dissolved in 15 mL of ether. The obtained dark brown solution was added with 15 mL of hexane, then the solvent excess was removed by a slow air flow (up to ~15 mL). The dark crystals formed (dark blue when ground) were filtered off, washed with hexane, and dried in air. Yield: 83%. M.p. 108 °C. The complex is soluble in most of organic solvents. On keeping in the solution for a day and longer, it gradually decomposes (in few minutes with low heating temperatures). During a long-term storage (more than 10 years) in the crystalline form, the complex gradually transforms into a complex with imino derivatives of this radical. Calculated for $C_{22}H_{21}N_4O_6F_{12}Cu$ (%): C 36.3, H 2.9, N 7.7, F 31.3. Found (%): C 37.0, H 3.1, N 7.6, F 31.3. This complex also forms when pure benzene or its mixtures with hexane (heptane) are used as solvents.

[$Cu(hfac)_2L^{Et/Et}$]. A mixture of $Cu(hfac)_2$ (0.0477 g, 0.1 mmol) and $L^{Et/Et}$ (0.0279 g, 0.10 mmol) samples was dissolved in 7 mL of hexane. The solvent excess was slowly removed by an air flow at room temperature to a volume of ~2 mL, after which the reaction mixture was cooled to –18 °C. Dark brown crystals formed in 36-38 h were filtered off and dried in air. Yield: 88%. M.p. 86-87 °C. Found (%): C 38.2, H 3.4, F 30.6, N 7.7. $C_{24}H_{25}CuF_{12}N_4O_6$. Calculated (%): C 38.1, H 3.3, F 30.1, N 7.4.

[$Cu(hfac)_2L^{Pr/Et}$]. A mixture of $Cu(hfac)_2$ (0.0477 g, 0.1 mmol) and mixtures of oil-like $L^{Pr/Et}$ and $L^{Pr/Et}$* (0.0300 g, 0.1 mmol) were dissolved in 2.5 mL of Et_2O and 4 mL of hexane were added. The reaction mixture was cooled to –30 °C. Large dark-red prismatic crystals formed in ~120 h were filtered off and dried in air. Yield: 77%. M.p. 81 °C. Found (%): C 39.1, H 3.1, F 30.5, N 7.4. $C_{25}H_{27}CuF_{12}N_4O_6$. Calculated (%): C 38.9, H 3.5, F 29.6, N 7.3.

[$Cu(hfac)_2L^{Me/Pr}$]. A mixture of $Cu(hfac)_2$ (0.0477 g, 0.1 mmol) and $L^{Me/Pr}$ (0.0280 g, 0.1 mmol) samples was dissolved in 4 mL of hexane at low heating temperatures (47 °C). The solution obtained was added with 0.5 mL of Et_2O. The reaction mixture was kept at room temperature for 1 h, after which it was cooled to +10 °C. Brown crystals formed in 24 h were filtered off and dried in air. Yield: 71%. M.p. 105-106 °C. Found (%): C 38.8, H 3.6, F 29.1, N 7.8. $C_{24}H_{25}CuF_{12}N_4O_6$. Calculated (%): C 38.1, H 3.3, F 30.1, N 7.4.

X-ray crystallography studies. Sets of reflections from single crystals of the compounds were collected on automated Bruker AXS - SMART APEX diffractometers (MoK_α radiation) with a Helix (Oxford Cryosystems) helium flow cooling system and Apex Duo (CuK_α radiation) with a Cobra (Oxford Cryosystems) cryosystem using the standard procedures. Structures were solved by direct methods and refined by the full-matrix least squares technique in the anisotropic approximation for non-hydrogen atoms. Hydrogen atoms are partially localized from the difference maps (the other were calculated geometrically) and included in the refinement in the riding model. All calculations were made using the SHELX software [14, 15]. Crystallographic characteristics of the studied compounds and experimental details are summarized in Tables 1-3. Full sets of the crystallographic data have been deposited with the Cambridge Crystallography Data Center (Tables 1-3).

Magnetic measurements. The magnetic susceptibility (χ) of the polycrystalline samples was measured on a Quantum Design MPMS*XL* SQUID-magnetometer in the temperature range of 2-300 K at the magnetic field strength of 5 kOe. Paramagnetic components of the magnetic susceptibility were determined with regard to a diamagnetic contribution

TABLE 1. Crystallographic Characteristics of the $[Cu(hfac)_2L^{Et/Et}]$ and Experimental Details

Parameter	Value				
Formula weight	757.02				
Space group	$P\bar{1}$				
Z	2				
T, K	295	250	200	150	103
a, Å	10.306(3)	10.3556(4)	10.3537(2)	10.3930(2)	10.4420(4)
b, Å	11.960(3)	11.8866(5)	11.8651(2)	11.8459(2)	11.8618(4)
c, Å	14.684(4)	14.5269(6)	14.3853(2)	14.1818(3)	13.9753(4)
α, deg	109.050(17)	109.215(3)	109.1890(10)	109.0660(10)	108.842(2)
β, deg	108.782(17)	108.702(2)	108.8550(10)	109.1120(10)	109.5040(10)
γ, deg	90.234(11)	90.301(3)	90.3350(10)	90.3730(10)	90.478(2)
V, Å^3	1607.6(8)	1587.07(12)	1566.99(5)	1546.61(5)	1531.08(9)
D_{cal}, g/cm^3	1.564	1.584	1.604	1.626	1.642
θ_{max}, deg	28.156	28.331	28.344	28.295	28.049
I_{hkl} measured / independent	27482 / 7747	28115 / 7780	28618 / 7761	26223 / 7580	24254 / 7269
R_{int}	0.0877	0.0505	0.0469	0.0534	0.0531
I_{hkl} ($I > 2\sigma_I$) / number of refined parameters	3111 / 526	4005 / 526	5228 / 526	4617 / 472	4718 / 481
$GOOF$	0.762	0.807	0.942	0.937	0.889
R_1 / wR_2 ($I > 2\sigma_I$)	0.0418 / 0.0869	0.0386 / 0.0821	0.0360 / 0.0868	0.0380 / 0.0755	0.0392 / 0.0863
R_1 / wR_2 (all data)	0.1216 / 0.1071	0.0935 / 0.0961	0.0587 / 0.0938	0.0801 / 0.0858	0.0704 / 0.0963
CCDC	2095859	2095854	2095858	2095852	2095851

TABLE 2. Crystallographic Characteristics of the $[Cu(hfac)_2L^{Me/Me}]$ and Experimental Details

Parameter	Value			
Formula weight	728.97			
Space group; Z	$P\bar{1}$; 2			
T, K	295	240	120	75
a, Å	10.0361(6)	9.9795(5)	9.8556(3)	9.790(2)
b, Å	11.5671(7)	11.4924(7)	11.4076(4)	10.931(2)
c, Å	14.9682(9)	14.9137(8)	14.7525(5)	14.626(3)
α, deg	70.670(4)	70.482(3)	70.535(2)	69.59(3)
β, deg	71.764(3)	71.915(3)	72.376(2)	71.08(3)
γ, deg	89.008(4)	89.954(3)	89.074(2)	87.64(3)
V, Å^3	1550.10(16)	1525.41(15)	1481.94(9)	1383.0(6)
d_{cal}, g/cm^3	1.562	1.587	1.634	1.750
θ_{max}, deg	28.195	28.053	28.189	23.286
I_{hkl} measured / independent	24372 / 7441	25770 / 7231	25861 / 7158	7183 / 3808
R_{int}	0.0499	0.0565	0.0473	0.0480
I_{hkl} ($I > 2\sigma_I$) / number of refined parameters	4414 / 517	4737 / 499	5188 / 528	2304 / 482
$GOOF$	0.901	0.983	1.095	0.993
R_1 / wR_2 ($I > 2\sigma_I$)	0.0386 / 0.0985	0.0407 / 0.1030	0.0399 / 0.1021	0.0550 / 0.1345
R_1 / wR_2 (all data)	0.0702 / 0.1089	0.0654 / 0.1115	0.0603 / 0.1090	0.1039 / 0.1624
CCDC	2095857	2095856	2095855	2095865

TABLE 3. Crystallographic Characteristics of the Compounds and Experimental Details

Parameter	$[Cu(hfac)_2L^{Me/Pr}]$			$[Cu(hfac)_2L^{Pr/Et}]$	$L^{Et/Et}$	$L^{Me/Pr}$
Formula weight	757.02			771.04	279.36	280.37
Space group; Z	$P\bar{1}$; 2			$P\bar{1}$; 2	$C2/c$; 8	Cc; 4
T, K	295	240	103	295	296	296
a, Å	10.9321(8)	10.7509(4)	10.5992(3)	9.7910(3)	31.19(2)	16.3360(11)
b, Å	11.4578(9)	11.3700(4)	11.2645(3)	12.8997(4)	9.325(8)	9.4849(6)
c, Å	14.0724(11)	13.8888(5)	13.6412(4)	14.7805(4)	11.600(9)	11.6270(14)
α, deg	109.887(5)	108.611(2)	108.190(2)	109.5920(10)	90	90
β, deg	102.217(5)	102.016(2)	101.725(2)	107.5990(10)	109.68(4)	119.313(4)
γ, deg	94.970(5)	95.286(2)	95.597(2)	90.335(2)	90	90
V, Å^3	1595.7(2)	1550.51(10)	1492.15(8)	1664.40(9)	3177(4)	1570.9(2)
d_{cal}, g/cm^3	1.576	1.621	1.685	1.539	1.168	1.185
θ_{max}, deg	27.997	28.600	28.160	28.353	30.553	28.489
I_{hkl} measured /	27103	26737	16678	28519	14027	5668
I_{hkl} independent	7574	7746	7172	8179	4652	3315
R_{int}	0.0486	0.0587	0.0503	0.0532	0.15981	0.0704
I_{hkl} ($I > 2\sigma_I$) / number of refined parameters	3285 / 544	4236 / 538	5542 / 474	4478 / 554	1055 / 182	1600 / 189
$GOOF$	0.807	0.855	0.993	0.870	0.902	0.773
R_1 ($I > 2\sigma_I$)	0.0353	0.0371	0.0337	0.0388	0.1106	0.0464
wR_2 ($I > 2\sigma_I$)	0.0762	0.0778	0.0836	0.0959	0.2589	0.0816
R_1 (all data)	0.1106	0.0802	0.0484	0.0782	0.3411	0.1045
wR_2 (all data)	0.0912	0.0872	0.0888	0.1063	0.3857	0.0963
CCDC	2095864	2095863	2095861	2095862	2095850	2095853

estimated from Pascal constants. The effective magnetic moment was calculated by the formula $\mu_{eff} = [3k\chi T / (N_A\mu_B^2)]^{1/2}$, where N_A, μ_B, and k are the Avogadro number, the Bohr magneton, and the Boltzmann constant respectively.

RESULTS AND DISCUSSION

The structure of nitroxides $L^{Me/Me}$, $L^{Et/Et}$, and $L^{Me/Pr}$, which we managed to obtain as single crystals suitable for the single crystal X-ray diffraction (XRD) analysis, is illustrated in Fig. 1. The same figure depicts the structures of $L^{Me/Et}$ and $L^{Et/Me}$ molecules, which are further used to compare the magnetic properties of individual NRs. The lengths of N–O bonds within 1.278(2)-1.284(2) Å, which is typical of nitronylnitroxide radicals [16-18]. Distances between the paramagnetic centers – O atoms of the neighboring molecules – exceed 4 Å. The introduction of the R2 substituent to the third position of the pyrazole ring causes a substantial turn of the pyrazole ring plane relative to the nitronylnitroxide fragment {ONCNO}. In monoalkyl-substituted spin-labeled pyrazoles L^{Me} and L^{Et}, this angle does not exceed 5° whereas in dialkylpyrazoles, it has a value larger than 30° (Table 4).

Results of studies of the magnetic properties of $L^{R1/R2}$ are illustrated in Fig. 2. High-temperature μ_{eff} values are well consistent with a theoretical purely spin value of 1.73 μ_B. For $L^{Me/Et}$ and $L^{Et/Me}$, when the temperature lowers, μ_{eff} first gradually decreases, and below 100 K this decrease is sharper. This behavior of the $\mu_{eff}(T)$ dependences indicates the occurrence of antiferromagnetic exchange interactions between NR spins. For $L^{Me/Pr}$ the μ_{eff} value remains constant on cooling to 5 K, and for $L^{Et/Et}$ some increase in μ_{eff} is observed below 30 K, which evidences the occurrence of ferromagnetic exchange interactions. Experimental $\mu_{eff}(T)$ dependences are well described within the model of exchange-bound dimers (spin Hamiltonian $H = -2J \cdot S_1S_2$). Optimal g-factors and exchange interaction parameters J are listed in Table 4. An increase in the size of substituents in the pyrazole ring leads to a decrease in the energy of exchange interactions between spins of nitroxides.

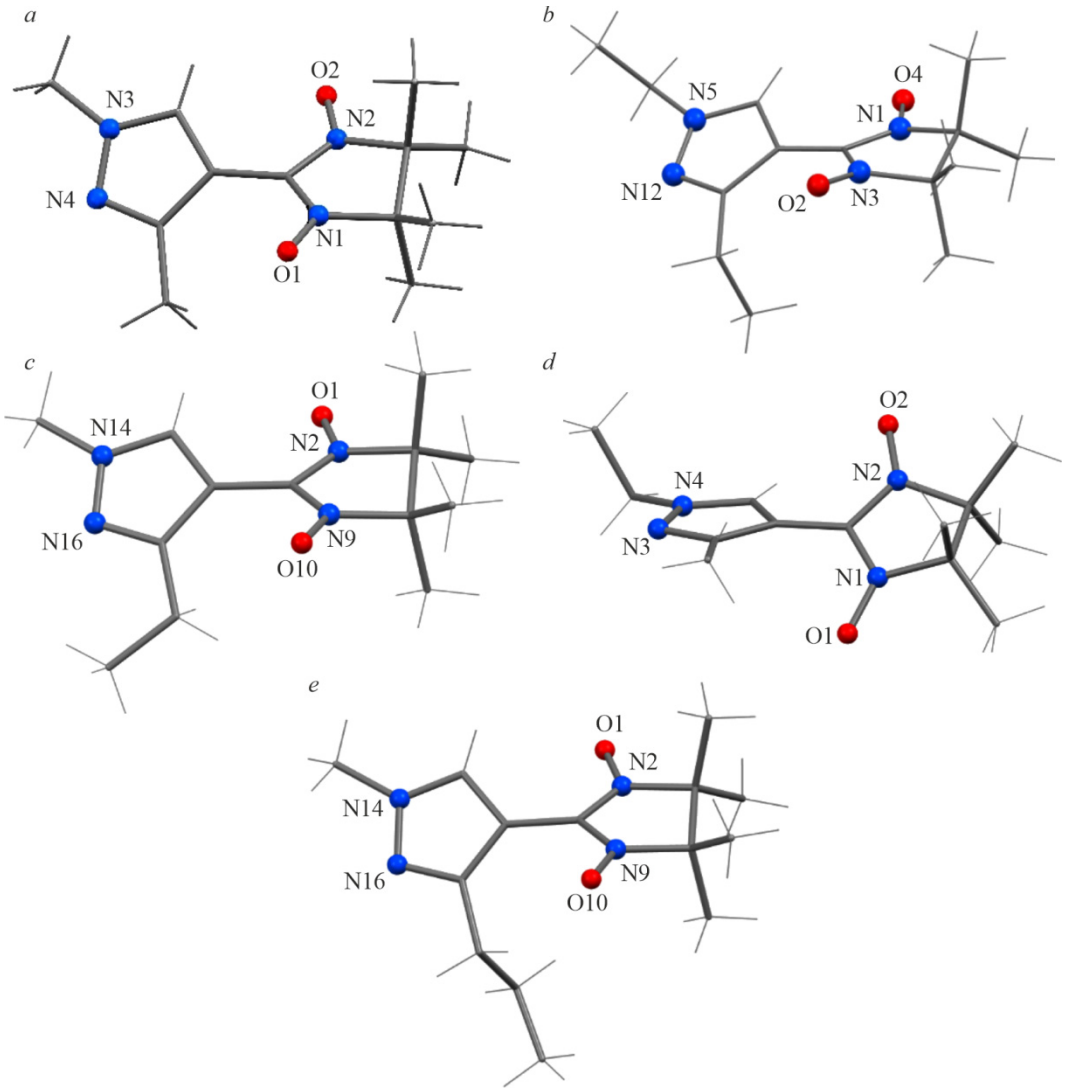

Fig. 1. Structures of $L^{Me/Me}$ (*a*), $L^{Et/Et}$ (*b*), $L^{Me/Et}$ (*c*), $L^{Et/Me}$ (*d*), and $L^{Me/Pr}$ (*e*) molecules.

TABLE 4. Selected Stereochemical NR Parameters, *g*-Factors, and the Exchange Interaction Energy *J*

Parameter	$L^{Me/Me}$ [12] [ECIGAY] [17]	$L^{Me/Et}$ [7]	$L^{Et/Me}$ [6] [GEMZOR] [17]	$L^{Et/Et}$	$L^{Me/Pr}$
T, K	296	296	296	296	296
N–O	1.283(2), 1.278(2)	1.289(3), 1.272(3)	1.293(2), 1.282(2), 1.287(2), 1.279(2)	1.280(6), 1.280(6)	1.289(3), 1.282(4)
$\angle CN_2O_2$–Pz	35.2	33.7	40.5, 39.9	31.9	37.7
$O_{NO}\ldots O_{NO}$	4.353(2)	4.187(3)	3.798(2)	4.002(5)	4.439(3)
g-factor	-	2.04(1)	2.06(1)	2.06(1)	2.04(1)
J, cm^{-1}	-	–5.6(1)	–16.3(1)	0.72(2)	–0.01(2)

All $[Cu(hfac)_2L^{R1/R2}]$ discussed below have a polymeric chain structure of the solid phase. The environment of all crystallographically independent Cu atoms is a centrosymmetric square bipyramid whose equatorial plane is formed by O_{hfac} atoms and axial positions are taken either by O_{NO} atoms of the nitronylnitroxide moiety or pyrazole N atoms (Fig. 3). Due to the bridging (ditopic) coordination of paramagnetic ligands there is an alternation of $\{CuO_4(O_{NO})_2\}$ and $\{CuO_4N_2\}$ coordination sites, which provides the general head-to-head motif of the chain (Fig. 3). The $\{CuO_4(O_{NO})_2\}$ sites are

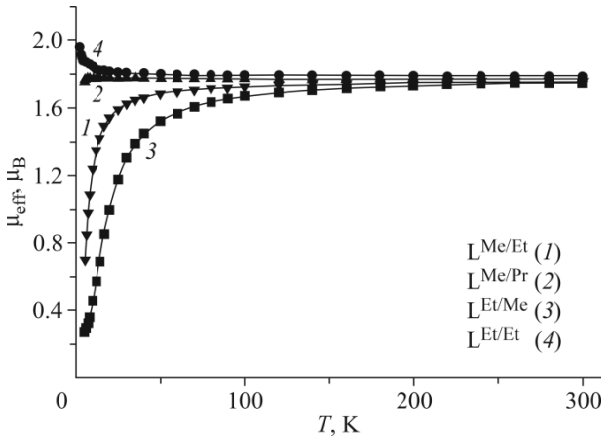

Fig. 2. Dependence $\mu_{eff}(T)$ for nitronylnitroxides $L^{R1/R2}$ (dots are the experimental values, solid lines are the theoretical curves).

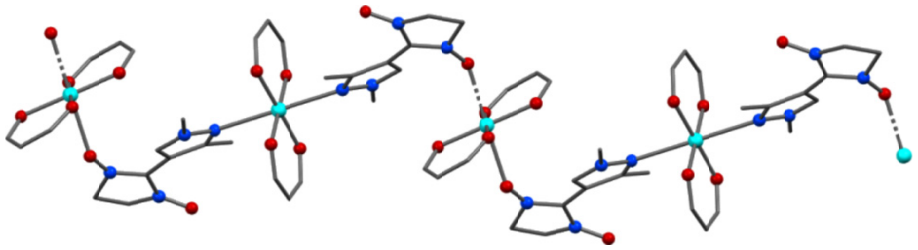

Fig. 3. Chain fragment in the $[Cu(hfac)_2L^{Me/Me}]$ structure.

heterospin exchange clusters {>N–•O–Cu^{2+}–O•–N<} with Cu–O_{NO} distances of 2.280(2)-2.360(1) Å at room temperature (Table 5). Here the second O_{NO} atom of the nitronylnitroxide moiety does not participate in the coordination and interchain distances between these atoms are longer than 3.9 Å.

The investigation of the magnetic properties reveals that for the $[Cu(hfac)_2L^{Me/Me}]$ complex the μ_{eff} value at 300 K is 2.57 μ_B (Fig. 4*a*). With decreasing temperature it gradually increases to 2.69 μ_B (at 90 K), after which it drops to 2.38 μ_B (at 83 K). On further cooling a small rise to 2.42 μ_B is observed (at 45 K) and again an abrupt decrease to 1.83 μ_B (at 35 K). Below 35 K the μ_{eff} value practically does not change and is close to the theoretical purely spin value of 1.86 μ_B for one paramagnetic center with spin $S = 1/2$ at a g-factor of 2.15.

The heating and cooling curves almost coincide, which indicates that the observed transitions are reversible. In the temperature range of 300-90 K, the $\mu_{eff}(T)$ dependence is described by the expression for the magnetic susceptibility with equal contributions from three-spin exchange clusters {>N–•O–Cu^{2+}–O•–N<} and isolated Cu^{2+} ions of the $\{CuO_4N_2\}$ coordination sites (Fig. 4*a*, curve *1*)

$$\chi = (\chi(J,T) + C/T)/2,$$

where $\chi(J,T) = \frac{N\mu_B^2}{3kT} \cdot \frac{15((g_{Cu}+2g_R)/3)^2 \cdot e^{J/kT} + 1.5((4g_R - g_{Cu})/3)^2 \cdot e^{-2J/kT} + 1.5g_{Cu}^2}{4 \cdot e^{J/kT} + 2 \cdot e^{-2J/kT} + 2}$ is the expression for the magnetic susceptibility of the three-spin exchange cluster (spin Hamiltonian $H = -2J(S_{R1}S_{Cu} + S_{Cu}S_{R2})$, $S_{R1} = S_{R2} = 1/2$ – NR spins). The magnetic susceptibility of isolated Cu^{2+} ions was taken into account using the Curie law $\chi = C/T$, where $C = N\mu_B^2(g_{Cu})^2 S(S+1)/3k \approx (g_{Cu})^2 S(S+1)/8$. Optimal g_{Cu} and J values are 2.09 cm^{-1} and 21.5 cm^{-1} (the value $g_R = 2$ was fixed to avoid reparametrization).

Drastic changes in the $\mu_{eff}(T)$ dependence are caused by structural transformations in heterospin clusters {>N–•O–Cu^{2+}–O•–N<}. Thus, a change in the nitroxide coordination from axial to equatorial gives rise to a strong antiferromagnetic

TABLE 5. Slected Bond Lengths, Intermolecular Contacts (Å), and Angles (deg) in $[Cu(hfac)_2(L^{R1/R2})]$

T, K	Cu–O_{NO}	Cu–N	∠CuON	N–O_{Cu}, N–O	O_{NO}…O_{NO}
			$[Cu(hfac)_2(L^{Me/Me})]$		
295	2.360(1)	2.546(2)	134.5(1)	1.290(2), 1.278(2)	3.971(3)
240	2.351(1)	2.521(2)	133.3(1)	1.286(2), 1.275(2)	3.916(2)
120	2.336(1)	2.466(2)	131.9(1)	1.287(2), 1.270(2)	3.838(2)
75	2.184(5)	2.415(6)	128.4(4)	1.259(7), 1.243(7)	3.774(7)
			$[Cu(hfac)_2(L^{Me/Pr})]$		
295	2.359(1)	2.651(2)	136.9(1)	1.289(2), 1.274(2)	3.980(3)
240	2.341(1)	2.650(2)	135.5(1)	1.290(2), 1.280(2)	3.781(3)
103	2.307(1)	2.598(1)	132.8(1)	1.294(2), 1.272(2)	3.643(2)
			$[Cu(hfac)_2(L^{Et/Et})]$		
295	2.280(2)	2.533(2)	132.8(1)	1.297(3), 1.269(3)	4.827(4)
250	2.247(2)	2.511(1)	131.8(1)	1.297(2), 1.272(2)	4.828(3)
200	2.198(1)	2.492(1)	130.4(1)	1.300(2), 1.276(2)	4.828(3)
150	2.109(1)	2.474(2)	128.4(1)	1.304(2), 1.271(2)	4.820(3)
103	2.020(1)	2.461(2)	127.0(1)	1.306(2), 1.277(2)	4.825(3)
			$[Cu(hfac)_2(L^{Pr/Et})]$		
295	2.338(1)	2.571(1)	133.1(1)	1.293(2), 1.279(2)	4.903(2)

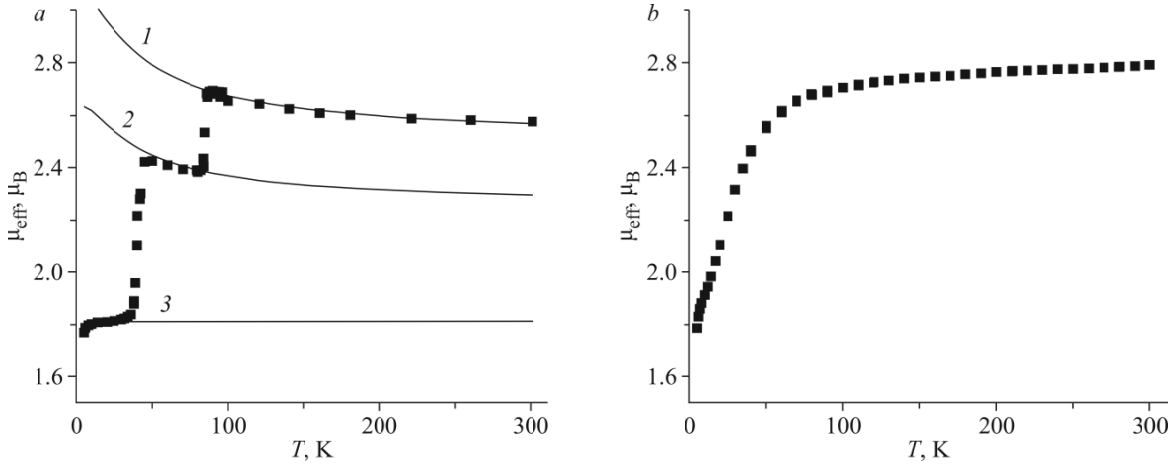

Fig. 4. Dependence $\mu_{eff}(T)$ for $[Cu(hfac)_2L^{Me/Me}]$ (*a*) and $[Cu(hfac)_2L^{Me/Pr}]$ (*b*) complexes; dots are the experimental data, solid lines (*1*, *2*, *3*) are the theoretical curves obtained as a result of modeling (comments in the text).

exchange between Cu^{2+} ion and NR spins and the compensation of a part of spins. The analysis of the $\mu_{eff}(T)$ dependence in the range of 85-45 K allows the estimation of a fraction of α clusters, in which a structural transition occurred, by the expression $\chi = ((1 - \alpha)\cdot\chi(J,T) + (1 + \alpha)\cdot C/T)/2$, using the values of g_{Cu} and J parameters for the high-temperature range. Changes in μ_{eff} at 85 K correspond to a transition of ~40% of heterospin clusters {>N–•O–Cu^{2+}–O•–N<} (α = 0.4, Fig. 4*a*, curve *3*). At 40 K a transition takes place in the rest of {CuO_6} coordination sites (α = 1, Fig. 4*a*, curve *3*).

For the $[Cu(hfac)_2L^{Me/Pr}]$ complex the $\mu_{eff}(T)$ dependence has another character (Fig. 4*b*). The μ_{eff} value of 2.79 μ_B at 300 K at first decreases gradually, and below 80 K there is an abrupt decrease reaching 1.78 μ_B at 5 K. The high-temperature μ_{eff} value corresponds to the theoretical purely spin value of 2.45 μ_B for two paramagnetic centers: one Cu(II) ion and

nitroxide with spins $S = 1/2$. The low-temperature μ_{eff} value corresponds to the theoretical purely spin value for one paramagnetic center with spin $S = 1/2$.

For $[Cu(hfac)_2L^{Et/Et}]$ the μ_{eff} value at 300 K is 2.65 μ_B (Fig. 5*a*), and decreases with temperature, reaching a plateau of ~1.84 μ_B below 80 K. The high-temperature μ_{eff} value corresponds to the theoretical purely spin value of 2.45 μ_B for two paramagnetic centers: one Cu^{2+} ion and NR with spins $S = 1/2$. The low-temperature μ_{eff} value is close to the theoretical purely spin value for one paramagnetic center with spin $S = 1/2$. The decrease in μ_{eff} in the temperature range of 300-80 K indicates the occurrence of a smooth spin transition and strong antiferromagnetic interactions in the low-temperature range for three-spin exchange clusters {>N–•O–Cu^{II}–O•–N<}, which are characteristic of the equatorial coordination of nitroxides. The analysis of the $\mu_{eff}(T)$ dependence below 130 K allows the estimation of the antiferromagnetic exchange interaction energy as $|J| > 85$ cm^{-1} at $g_{Cu} = 2.3$. In the room temperature range, the $\mu_{eff}(T)$ dependence approaches the theoretical curve with g_{Cu} and J parameters of 2.3 cm^{-1} and 14 cm^{-1}, which corresponds to weak ferromagnetic interactions in three-spin exchange clusters {>N–•O–Cu^{II}–O•–N<} that are characteristic of the axial coordination of nitroxides. For comparison we present the theoretical curve with g_{Cu} and J parameters of 2.3 cm^{-1} and –14 cm^{-1}, which corresponds to weak antiferromagnetic exchange.

For the $[Cu(hfac)_2L^{Pr/Et}]$ complex the $\mu_{эeff}$ value at 300 K is 2.55 μ_B and with decreasing temperature it at first decrease gradually and below 150 K it decreases abruptly (Fig. 5*b*), reaching 2.27 μ_B at 80 K. Below 80 K there is an increase in μ_{eff} to 2.42 μ_B at 7 K, which reveals the occurrence of ferromagnetic exchange interactions. The analysis of the $\mu_{eff}(T)$ dependence in the temperature range of 5-80 K allows the estimation of the exchange interaction energy and a fraction of heterospin clusters {>N–•O–Cu^{2+}–O•–N<} with the equatorial coordination of nitroxides, and consequently, with strong antiferromagnetic exchange. Optimal values of g_{Cu} and J parameters are 2.14 cm^{-1} and 9.7 cm^{-1} at a fixed value $\alpha = 0.5$ (Table 5*b*, curve *3*). Theoretical curve *1* corresponds to the value $\alpha = 1$ at the same g_{Cu} and J parameters (2.14 cm^{-1} and 9.7 cm^{-1}), and in the high-temperature range it approaches the experimental μ_{eff} values. In the temperature range of 300-150 K, the experimental $\mu_{eff}(T)$ dependence is well described by a curve with g_{Cu} and J parameters of 2.24 cm^{-1} and –16.4 cm^{-1} at $\alpha = 1$ (Fig. 5*b*, curve *2*).

In $[Cu(hfac)_2L^{R1/R2}]$ crystal structures, the polymeric chains are packed similarly (Fig. 6), and the interchain $O_{NO}…O_{NO}$ distances between uncoordinated atoms are sufficiently long (Table 5), therefore, the observed distinctions in the temperature dynamics of magnetic properties are first of all caused by the features of changes in the structure of the complex inside the chains.

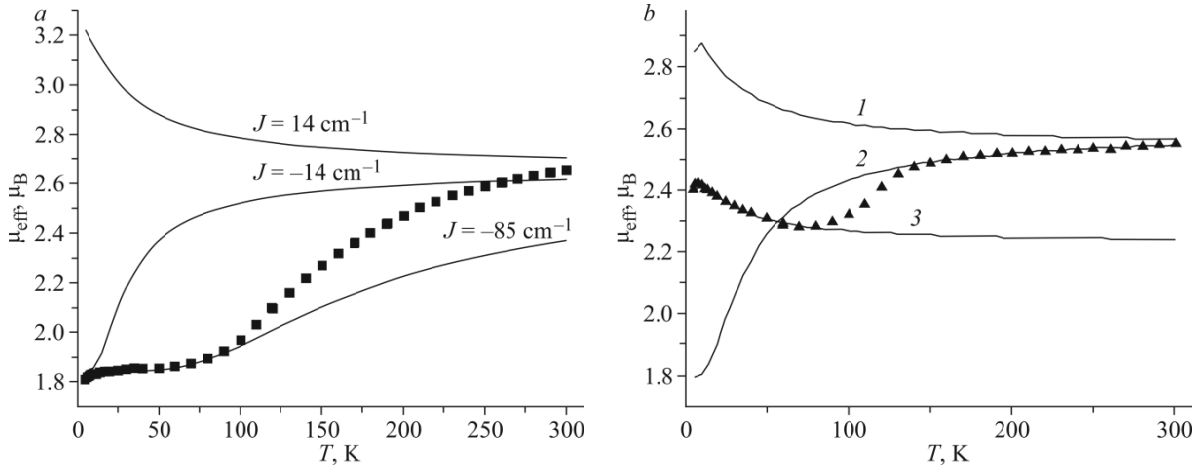

Fig. 5. Dependence $\mu_{eff}(T)$ for $[Cu(hfac)_2L^{Et/Et}]$ (*a*) and $[Cu(hfac)_2L^{Pr/Et}]$ (*b*) complexes; dots are the experimental data, solid lines (*1*, *2*, *3*) are the theoretical curves obtained as a result of modeling (comments in the text).

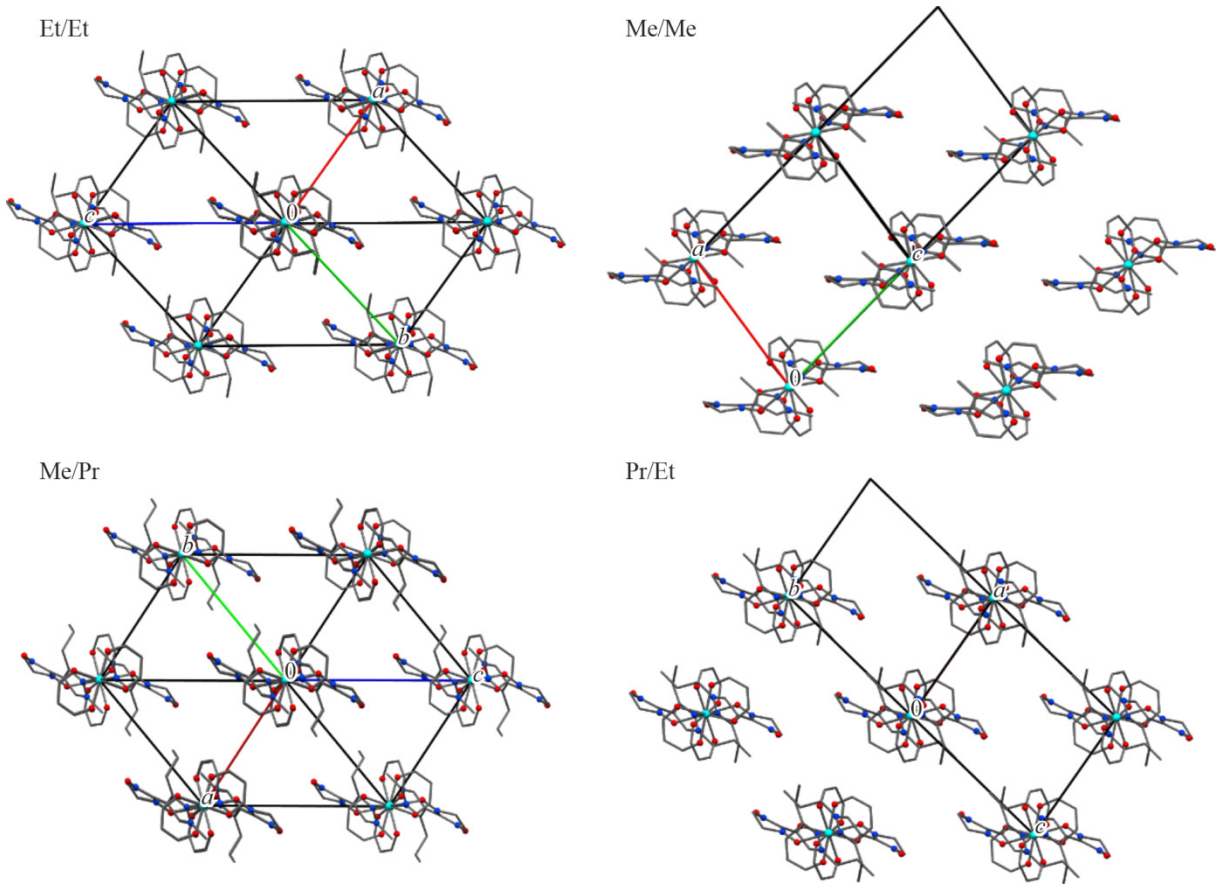

Fig. 6. Packing of polymeric chains of $[Cu(hfac)_2L^{R1/R2}]$ complexes in the crystal.

A series of low-temperature single crystal XRD studies of $[Cu(hfac)_2(L^{Me/Me})]$ has shown that upon cooling from 300 K to 120 K the environment of the Cu atom changes insignificantly: the Cu–O_{NO} bond length decreases only by 0.024 Å (from 2.360 Å to 2.336 Å). Then at 75 K it reduces immediately by 0.152 Å (Table 5), i.e. there is a tendency to replace elongated Jahn Teller's axis O_{NO}–Cu–O_{NO} by O_{hfac}–Cu–O_{hfac} in the Cu atom environment in the {CuO6} coordination site. We failed to trace structural changes below this temperature because of crystal fracturing.

The comparison of $[Cu(hfac)_2(L^{Me/Me})]$ and $[Cu(hfac)_2(L^{Me/Pr})]$ structures revealed the similar structures of their fragments and chain packings as well as changes in their structures with decreasing temperature from 300 K to 100 K. A significant distinction was found in Cu–N distances at $\{CuO_4N_2\}$ sites: in $[Cu(hfac)_2(L^{Me/Pr})]$ it is larger by 0.1 Å and practically remains unchanged when the crystal is cooled. This is likely to be due to the location of the Pr-substituent in a limited space between hfac ligands of this site and the uncoordinated NR fragment (Fig. 7), which does not allow the Cu and O_{NO} atoms to approach at a distance required for the spin transition. It is also worth noting an appreciable decrease in the distances between NRs of the neighboring O_{NO}…O_{NO} chains by на 0.35 Å in the temperature range of 295-103 K (Table 5), which results in strengthening antiferromagnetic interactions between them and causes a decrease in the μ_{eff} value at temperatures below 80 K.

The structural feature of $[Cu(hfac)_2L^{Et/Et}]$ and $[Cu(hfac)_2L^{Pr/Et}]$ is the location of terminal groups of alkyl substituents on one side of the pyrazole ring (in free $L^{Et/Et}$ they are on different sides, Fig 1). In its polymeric chain at 295 K, the Cu–O_{NO} distances in the $\{CuO_6\}$ sites (Table 5) are the shortest among all $[Cu(hfac)_2L^{Et/R2}]$ with the head-to-head motif. When the temperature lowers from 295 K to o 103 K, their smooth shortening is detected from 2.279(2) Å to 2.020(1) Å, i.e. in {CuO6} sites, the elongated Jahn-Teller axis changes from O_{NO}–Cu–O_{NO} to O_{hfac}–Cu–O_{hfac}. This corresponds to a decrease in the μ_{eff} value due to strengthening exchange interactions of the antiferromagnetic character in these sites (Fig. 5*a*). As shown

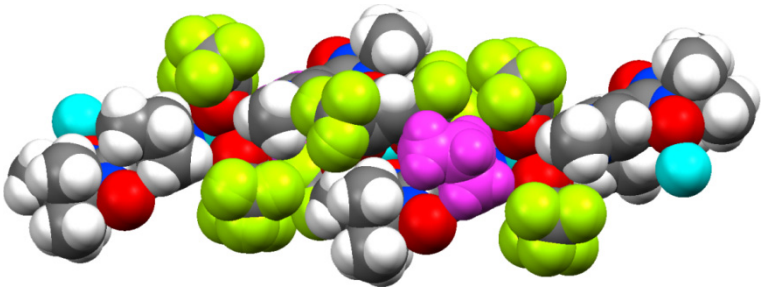

Fig. 7. [Cu(hfac)$_2$(L$^{Me/Pr}$)] chain fragment at $T = 103$ K in the space-filling representation; Pr-substituent atoms are shown by crimson (see electronic version).

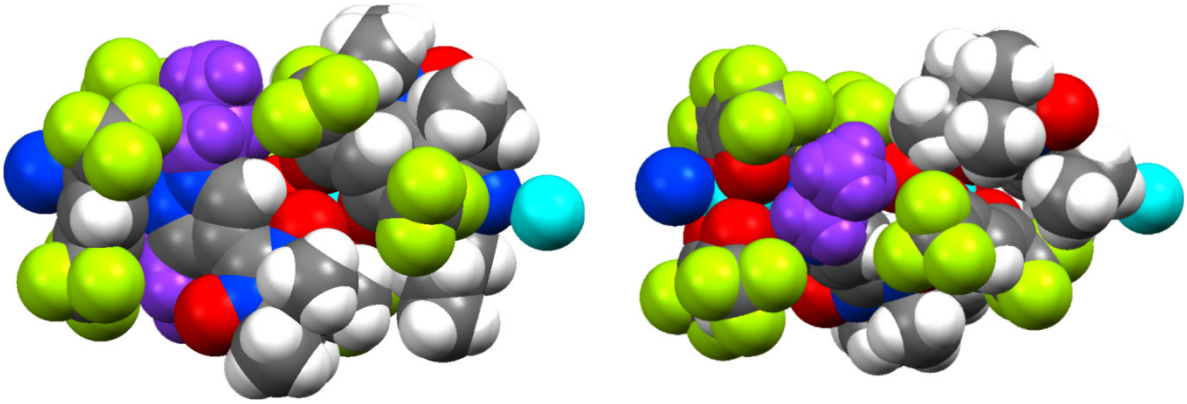

Fig. 8. [Cu(hfac)$_2$(L$^{Pr/Et}$)] chain fragments in the space-filling representation; atoms of alkyl substituents are shown by purple (see electronic version).

previously by quantum chemical calculations, this effect is a consequence of a decrease in the fraction of a low-temperature phase in the structure of the high-temperature phase with decreasing temperature [19-21].

The [Cu(hfac)$_2$L$^{Pr/Et}$] single crystals turned to be thermally inelastic and decomposed when cooled. Therefore, we failed to trace changes in distances in solid KC upon its cooling. As can be seen in Fig. 8, two bulky substituents in L$^{Pr/Et}$, which are located between hfac ligands and the uncoordinated nitroxide fragment, certainly should hinder the displacement of chain fragment when the crystal is cooled.

CONCLUSIONS

Thus, the comparison of the structure and the temperature structure dynamics of [Cu(hfac)$_2$L$^{Me/Me}$], [Cu(hfac)$_2$L$^{Et/Et}$], [Cu(hfac)$_2$L$^{Me/Pr}$], [Cu(hfac)$_2$L$^{Pr/Et}$] heterospin complexes with [Cu(hfac)$_2$L$^{Me/H}$], [Cu(hfac)$_2$L$^{Et/H}$], [Cu(hfac)$_2$L$^{Pr/H}$], [Cu(hfac)$_2$L$^{Et/Me}$], and [Cu(hfac)$_2$L$^{Me/Et}$] previously described for complexes with mono- and dialkyl-substituted spin-labeled pyrazoles has shown that changes of both R1 and R2 substituents can significantly affect not only the possibility of the appearance of anomalies in the temperature dependence curve of the effective magnetic moment but also its form.

FUNDING

The work was supported by the Russian Science Foundation (grant No.17-13-01022) and RFBR in the synthesis of the compounds (grant No. 18-29-04002).

CONFLICT OF INTERESTS

The authors declare that they have no conflict of interests.

REFERENCES

1. V. Ovcharenko. In: Stable Radicals / Ed. R. Hicks. Chichester, UK: John Wiley & Sons, Ltd, **2010**, 461-506. https://doi.org/10.1002/9780470666975.ch13
2. V. Ovcharenko and E. Bagryanskaya. In: Spin-Crossover Mater / Ed. M. A. Halcrow. Oxford, UK: John Wiley & Sons Ltd, **2013**, 239-280. https://doi.org/10.1002/9781118519301.ch9
3. N. A. Artiukhova, G. V. Romanenko, A. S. Bogomyakov, I. Y. Barskaya, S. L. Veber, M. V. Fedin, K. Y. Maryunina, K. Inoue, and V. I. Ovcharenko. *J. Mater. Chem. C*, **2016**, *4*, 11157-11163. https://doi.org/10.1039/C6TC03216H
4. S. V. Fokin, E. T. Kostina, E. V. Tret′yakov, G. V. Romanenko, A. S. Bogomyakov, R. Z. Sagdeev, and V. I. Ovcharenko. *Russ. Chem. Bull.*, **2013**, *62*, 661-671. https://doi.org/10.1007/s11172-013-0089-y
5. S. E. Tolstikov, N. A. Artiukhova, G. V. Romanenko, A. S. Bogomyakov, E. M. Zueva, I. Y. Barskaya, M. V. Fedin, K. Y. Maryunina, E. V. Tretyakov, R. Z. Sagdeev, and V. I. Ovcharenko. *Polyhedron*, **2015**, *100*, 132-138. https://doi.org/10.1016/j.poly.2015.07.029
6. V. I. Ovcharenko, S. V. Fokin, E. T. Kostina, G. V. Romanenko, A. S. Bogomyakov, and E. V. Tretyakov. *Inorg. Chem.*, **2012**, *51*, 12188-12194. https://doi.org/10.1021/ic301328x
7. V. Ovcharenko, S. Fokin, E. Chubakova, G. Romanenko, A. Bogomyakov, Z. Dobrokhotova, N. Lukzen, V. Morozov, M. Petrova, M. Petrova, G. Levkovskaya, and R. Sagdeev. *Inorg. Chem.*, **2016**, *55*, 5853-5861. https://doi.org/10.1021/acs.inorgchem.6b00140
8. K. Y. Maryunina, X. Zhang, S. Nishihara, K. Inoue, V. A. Morozov, G. V. Romanenko, and V. I. Ovcharenko. *J. Mater. Chem. C*, **2015**, *3*, 7788-7791. https://doi.org/10.1039/C5TC01005E
9. V. Ovcharenko, G. Romanenko, A. Polushkin, G. Letyagin, A. Bogomyakov, M. Fedin, K. Maryunina, S. Nishihara, K. Inoue, M. Petrova, V. Morozov, and E. Zueva. *Inorg. Chem.*, **2019**, *58*, 9187-9194. https://doi.org/10.1021/acs.inorgchem.9b00815
10. E. T. Chubakova. Sintez, stroenie i svoistva geyerospinovykh kompleksov bis(geksaftoratsetilatsetonato) medi(II) s novymi pirazolil-zameshchennymi nitroksil'nymi radikalami (Synthesis, Structure, and Properties of Heterospin Complexes of bis(Hexafluoroacetylacetonato) Copper(II) with New Pyrasolyl-Substituted Nitroxide Radicals): Cand. (Chem.) Dissertation. Novosibirsk: Nikolaev Institute of Inorganic Chemistry, **2014**. [In Russian]
11. V. I. Ovcharenko, S. V. Fokin, G. V. Romanenko, I. V. Korobkov, and P. Rey. *Russ. Chem. Bull.*, **1999**, *48*, 1519-1525. https://doi.org/10.1007/BF02496404
12. G. V. Romanenko, S. V. Fokin, S. F. Vasilevskii, E. V. Tret′yakov, Y. G. Shvedenkov, and V. I. Ovcharenko. *Russ. J. Coord. Chem.*, **2001**, *27*, 360-367. https://doi.org/10.1023/A:1011354314831
13. V. Ovcharenko, S. Fokin, E. Chubakova, G. Romanenko, A. Bogomyakov, Z. Dobrokhotova, N. Lukzen, V. Morozov, M. M. Petrova, M. M. Petrova, E. Zueva, I. Rozentsveig, E. Rudyakova, G. Levkovskaya, and R. Sagdeev. *Inorg. Chem.*, **2016**, *55*, 5853-5861. https://doi.org/10.1021/acs.inorgchem.6b00140
14. G. M. Sheldrick. *Acta Crystallogr.*, *Sect. A: Found. Adv.*, **2015**, *71*, 3-8. https://doi.org/10.1107/S2053273314026370
15. G. M. Sheldrick. *Acta Crystallogr.*, *Sect. C: Struct. Chem.*, **2015**, *71*, 3-8. https://doi.org/10.1107/S2053229614024218
16. E. V. Tretyakov and V. I. Ovcharenko. *Russ. Chem. Rev.*, **2009**, *78*, 971-1012. https://doi.org/10.1070/RC2009v078n11ABEH004093
17. C. R. Groom, I. J. Bruno, M. P. Lightfoot, and S. C. Ward. *Acta Crystallogr.*, *Sect. B: Struct. Sci. Cryst. Eng. Mater.*, **2016**, *72*, 171-179. https://doi.org/10.1107/S2052520616003954

18. S. Fokin, V. Ovcharenko, G. Romanenko, and V. Ikorskii. *Inorg. Chem.*, **2004**, *43*, 969-977. https://doi.org/10.1021/ic034964d
19. E. M. Zueva, E. R. Ryabykh, and A. M. Kuznetsov. *Russ. Chem. Bull.*, **2009**, *58*, 1654-1662. https://doi.org/10.1007/s11172-009-0228-7
20. V. I. Ovcharenko, G. V. Romanenko, K. Y. Maryunina, A. S. Bogomyakov, and E. V. Gorelik. *Inorg. Chem.*, **2008**, *47*, 9537-9552. https://doi.org/10.1021/ic8011074
21. V. A. Morozov, M. V. Petrova, and N. N. Lukzen. *AIP Adv.*, **2015**, *5*, 087161. https://doi.org/10.1063/1.4929526